Noise control in enclosures: Modeling and experiments with T-shaped acoustic resonators

D. Li, L. Cheng,[a] and G. H. Yu
Department of Mechanical Engineering, The Hong Kong Polytechnic University, Hung Hom, Kowloon, Hong Kong, SAR of China

J. S. Vipperman
Department of Mechanical Engineering and Materials Science, University of Pittsburgh, Pittsburgh, Pennsylvania 15261

(Received 10 January 2007; revised 13 August 2007; accepted 14 August 2007)

This paper presents a theoretical and experimental study of noise control in enclosures using a T-shaped acoustic resonator array. A general model with multiple resonators is developed to predict the acoustic performance of small resonators placed in an acoustic enclosure. Analytical solutions for the sound pressure inside the enclosure and the volume velocity source strength out of the resonator aperture are derived when a single resonator is installed, which provides insight into the physics of acoustic interaction between the enclosure and the resonator. Based on the understanding of the coupling between the individual resonators and enclosure modes, both targeted and nontargeted, a sequential design methodology is proposed for noise control in the enclosure using an array of acoustic resonators. Design examples are given to illustrate the control performance at a specific or at several resonance peaks within a frequency band of interest. Experiments are conducted to systematically validate the theory and the design method. The agreement between the theoretical and experimental results shows that, with the help of the presented theory and design methodology, either single or multiple resonance peaks of the enclosure can be successfully controlled using an optimally located acoustic resonator array. © *2007 Acoustical Society of America.* [DOI: 10.1121/1.2783122]

PACS number(s): 43.50.Gf, 43.50.Jh, 43.20.Ks [KA] Pages: 2615–2625

I. INTRODUCTION

Enclosures are widely used in civil and industrial systems. Typical examples, such as cabinets of ground vehicles, nacelles of helicopters, and payload fairings of launch vehicles, exhibit a commonality of having relatively compact interior dimensions. Low-frequency noise problems in such small enclosures are difficult to deal with since only compact noise control devices can satisfy the spatial limitations. When properly designed, a passive method using an acoustic resonator can effectively absorb acoustic energy from a targeted acoustic mode.[1–9] Ideally, it is desirable to integrate resonators into the host structure to save space, particularly for small enclosures. However, it is difficult to meet this requirement with a classical Helmholtz resonator because of its bulbous profile. In order to overcome the drawbacks of conventional resonators, considerable effort has been devoted to developing new ideas and solutions.[10] A good example is the recent work by Li and Vipperman,[7,8,11] who developed a multimodal design theory of a long T-shaped acoustic resonator (TAR) for the low-frequency noise transmission control in an expendable launch vehicle (ELV) payload fairing. A TAR consists of two mutually perpendicular tubes: a long closed-end tube and a short open-end tube. Compared with conventional Helmholtz resonators, one of the biggest advantages offered by the TAR is its large aspect ratio. This unique feature makes it possible to integrate a TAR into the host structure as a structural component, such as a beam, a pillar, or an enhanced rib, which relaxes the space requirement in the implementation. In the previous work, a TAR array has been structurally integrated into an ELV payload fairing, resulting in a 6–9 dB noise reduction in noise transmission control.[7,8]

Various theoretical and experimental studies on the acoustic interaction between an enclosure and conventional Helmhotz resonators have been reported in the literature. Fahy and Schofield presented a theoretical model involving acoustic interaction between an enclosure and a single Helmholtz resonator,[12] which provides early explicit insight into the fundamental physics of the acoustic interaction. Later, Cummings developed a multimodal theory to deal with the acoustic coupling problem when introducing a Helmholtz or quarter-wave resonator array into the enclosure.[13] Each resonator was modeled as a secondary point source with an unknown volume velocity. The problem was approached by equalizing the pressure at each resonator aperture, which was computed from knowledge of the acoustic impedance of the resonators, and the pressure at the same location, which was determined from the radiation of the primary and secondary sound sources. Thus, a singularity problem was reported when calculating the pressure at the resonator aperture using the volume velocity of the resonator itself.[13] In order to solve the problem, an average sound pressure at the surface of an equivalent small pulsating sphere was used as the pressure at

[a]Electronic mail: mmlcheng@polyu.edu.hk

the resonator aperture. This approximation can prevent the singularity problem but at the expense of introducing other problems. For example, it was found that the coupled frequencies predicted from the sphere-based model were different from the measured ones. Recently, a vibroacoustic coupling model was presented by Estève and Johnson to control noise transmitted into a composite cylinder using distributed vibration absorbers and Helmholtz resonators.[2,3] Noise control using long cylindrical tube-shaped resonators for fairing noise control has also been investigated.[4,5]

Despite all the effort, the design of acoustic resonators is still limited by a number of factors. The first one is the lack of theoretical modeling tools to facilitate and optimize the design of such devices for a given enclosure, which actually still involves intensive experimental measurements on a trial-and-error basis. Moreover, should more resonators be used to form a resonator array to increase the control performance inside a small enclosure, an effective design cannot be achieved without considering the acoustic coupling between the resonators and all acoustic modes of the enclosure, as suggested by the earlier observation on conventional Helmholtz resonators.[12]

This paper attempts to provide a theoretical model to predict the acoustic performance of multiple resonators placed in an acoustic enclosure, along with a reliable design methodology to maximize the control performance. In a broader perspective, the general model is applicable not only to the TAR, but also to classical Helmholtz resonators. The paper is divided into four sections. The general model is first presented in Sec. II. The formulation is based on the modal expansion of pressure in the enclosure and its coupling to the resonators. Acoustic output impedance is used to package the dynamic information of the TAR, which greatly simplifies the modeling process. A special case (with one resonator installed) is selected for detailed analysis, and a sequential design method (SDM) is also proposed in this section. Numerical simulations and experimental validations are performed in Sec. III. A detailed implementation procedure using a TAR array to control a single or multiple resonance peaks is demonstrated and discussed. Experimental validations are systematically carried out for each important stage of development, including the evaluation of dissipation characteristics of resonators, the performance assessment of the SDM with multiple resonators, and the validation of optimal locations of resonators. Finally, conclusions are drawn in the last section.

II. THEORY

In the following, a general model considering acoustic interaction between an enclosure and an acoustic resonator array is developed before the special case involving a single resonator is discussed. Throughout the paper, the superscripts and subscripts E, R, and S stand for variables associated with "enclosure," "resonator," and "primary source," respectively.

A. Acoustic interaction between enclosure and acoustic resonator array

The inhomogeneous wave equation governing the pressure fields inside the enclosure is

$$\nabla^2\phi(\mathbf{r},t) - \frac{1}{c^2}\ddot{\phi}(\mathbf{r},t) = q(\mathbf{r},t), \tag{1}$$

where $\phi(\mathbf{r},t)$ is the acoustic velocity potential; c the sound speed; and q the volume velocity source strength density distribution within the volume or on the surface of the enclosure. Assuming that a set of N harmonic sources with volume velocity source strength density $q_1^S, q_2^S, \ldots, q_N^S$ located at the points $\mathbf{r}_1^S, \mathbf{r}_2^S, \ldots, \mathbf{r}_N^S$ form the primary sound field, and M resonators with volume velocity source strength density $q_1^R, q_2^R, \ldots, q_M^R$ located at the points $\mathbf{r}_1^R, \mathbf{r}_2^R, \ldots, \mathbf{r}_M^R$ (centers of the resonator apertures) form the secondary sound field in the enclosure, Eq. (1) becomes

$$\nabla^2\phi(\mathbf{r},t) - \frac{1}{c^2}\ddot{\phi}(\mathbf{r},t) = \sum_{m=1}^{M} q_m^R(t)\,\delta(\mathbf{r}-\mathbf{r}_m^R) + \sum_{n=1}^{N} q_n^S(t)\,\delta(\mathbf{r}-\mathbf{r}_n^S), \tag{2}$$

where $\delta(\mathbf{r}-\mathbf{r}_0)$ is a three-dimensional Dirac delta function. Notice that the volume velocity out of the resonator has the same sign as that of the primary sound source, i.e., the positive sign is directed out of the source into the enclosure, which results in an opposite sign as compared to that defined in many textbooks.[14,15] The volume velocity source strength density out of the acoustic resonator can be computed from

$$Z_m = \frac{p(\mathbf{r},t)\,\delta(\mathbf{r}-\mathbf{r}_m^R)}{q_m^R(t)}, \tag{3}$$

where Z_m is defined as the acoustic output impedance at the aperture of the mth resonator, and $p(\mathbf{r}_m^R,t)$ is the sound pressure at $\mathbf{r}_m^R$ provided the largest dimension of the resonator aperture is smaller than the sound wavelength of interest. Substituting Eq. (3) into Eq. (2) and using $p(\mathbf{r},t) = -\rho_0\dot{\phi}(\mathbf{r},t)$, Eq. (2) becomes

$$\nabla^2\phi(\mathbf{r},t) - \frac{1}{c^2}\ddot{\phi}(\mathbf{r},t) = -\rho_0\sum_{m=1}^{M}\frac{\dot{\phi}(\mathbf{r},t)\,\delta(\mathbf{r}-\mathbf{r}_m^R)}{Z_m} + \sum_{n=1}^{N} q_n^S(t)\,\delta(\mathbf{r}-\mathbf{r}_n^S). \tag{4}$$

Acoustic velocity potential $\phi(\mathbf{r},t)$ can be decomposed on the basis of the respective mode-shape functions of the enclosure: $\phi(\mathbf{r},t) = \Sigma\psi_j(t)\varphi_j(\mathbf{r})$, where $\psi_j(t)$ is the jth modal response and $\varphi_j(\mathbf{r})$ is the jth eigenfunction given in Ref. 13. Substituting this modal expansion into Eq. (4) and applying orthogonality properties of the eigenfunctions yields an uncoupled acoustic equation,

$$\ddot{\psi}_j(t) - \frac{cz_0}{V^E}\sum_{h=1}^{J}\left\{\sum_{m=1}^{M}\left[\frac{1}{Z_m}\frac{\varphi_j(\mathbf{r}_m^R)\varphi_h(\mathbf{r}_m^R)}{\Lambda_j}\right]\dot{\psi}_h(t)\right\} + (\gamma_j^E)^2\psi_j(t) = -\frac{c^2}{V^E}\sum_{n=1}^{N}\frac{\tilde{\varphi}_j(\mathbf{r}_n^S)}{\Lambda_j}q_n^S(t), \tag{5}$$

where j and $h=1,2,3,\ldots,J$ are the indices of the modal response, $z_0=\rho_0 c$ is the characteristic acoustic impedance of the fluid, V^E is the volume of the enclosure, $\Lambda_j = \int_{V^E}[\varphi_j(\mathbf{r})]^2 dV/V^E$ is the modal normalization factor, $\tilde{\varphi}_j(\mathbf{r}_n^S)$ is the averaged $\varphi_j(\mathbf{r}_n^S)$ over the volume of the nth source, and γ_j^E is the jth complex eigenvalue of the enclosures, expressed as $\gamma_j^E=\omega_j^E+iC_j^E$, in which the real part is the angular frequency and the imaginary part is an equivalent *ad hoc* damping coefficient.

Assuming all time-dependent variables are harmonic, i.e., $\psi_j(t)=P_j e^{i\omega t}$ and $q_n^S(t)=Q_n^S e^{i\omega t}$, Eq. (5) becomes

$$\left[\frac{\omega^2-(\gamma_j^E)^2}{\omega^2}+i\frac{z_0}{kV^E}\sum_{m=1}^{M}\frac{1}{Z_m}\frac{[\varphi_j(\mathbf{r}_m^R)]^2}{\Lambda_j}\right]\frac{P_j}{\frac{Q^s}{k^2V^E}} + i\frac{z_0}{kV^E}\sum_{h\neq j}^{J}\left[\sum_{m=1}^{M}\frac{1}{Z_m}\frac{\varphi_j(\mathbf{r}_m^R)\varphi_h(\mathbf{r}_m^R)}{\Lambda_j}\right]\frac{P_h}{\frac{Q^s}{k^2V^E}} = \sum_{n=1}^{N}\frac{\tilde{\varphi}_j(\mathbf{r}_n^S)}{\Lambda_j}\frac{Q_n^S}{Q^s}, \tag{6}$$

where Q^S is the volume velocity source strength of any point source, and k is the wave number. When a finite number of enclosure modes are considered, Eq. (6) forms a set of linear equations. The set of linear equations can be numerically solved with the modal response coefficients $P_j/(Q^S/k^2V^E)$ as unknowns if the eigenfunctions and eigenvalues of the enclosure are given. A dimensionless amplitude of sound pressure inside the enclosure can be then computed from $p(\mathbf{r},t)=-\rho_0\dot{\phi}(\mathbf{r},t)$ as

$$\frac{p(\mathbf{r})}{\frac{i\omega\rho_0 Q^S}{k^2V^E}} = -\sum_{j=1}^{J}\left[\varphi_j(\mathbf{r})\left(\frac{P_j}{\frac{Q^S}{k^2V^E}}\right)\right]. \tag{7}$$

A dimensionless sound pressure level (SPL) is used to evaluate the pressure distribution inside the enclosure as

$$L_p(\mathbf{r}) = 20\log\left|\frac{p(\mathbf{r})}{\frac{i\omega\rho_0 Q^S}{k^2V^E}}\right|. \tag{8}$$

B. Acoustic interaction between an enclosure and a single TAR

In a previous study,[12] the targeted enclosure mode by a single resonator was assumed to be well separated in frequency from other neighboring modes, such that only the targeted mode was taken into account in the analysis of acoustic interaction. For enclosures with higher modal density, however, the neighboring acoustic modes are not well separated, such that a general model accounting for all enclosure modes is needed. In the following, such a model, namely the acoustic interaction between one single resonator and the enclosure with multiple modes, is introduced. This analysis results in analytical solutions of the sound pressure inside the enclosure and the volume velocity source strength from the resonator aperture, which provide insight into the fundamental physics of the acoustic interaction between the primary and the secondary sound sources.

With one acoustic resonator and N point sources in the enclosure, the acoustic equation in the enclosure can be obtained from Eq. (6) after eliminating subscript m,

$$[\omega^2-(\gamma_j^E)^2]P_j + i\frac{cz_0\omega}{V^E}\frac{1}{Z}\sum_{h=1}^{J}\frac{\varphi_j(\mathbf{r}^R)\varphi_h(\mathbf{r}^R)}{\Lambda_j}P_h = \frac{c^2}{V^E}\sum_{n=1}^{N}\frac{\tilde{\varphi}_j(\mathbf{r}_n^S)}{\Lambda_j}Q_n^S. \tag{9}$$

The modal response of P_j can be solved from Eq. (9) as

$$\frac{P_j}{\frac{Q^S}{k^2V^E}} = \underbrace{\frac{\omega^2}{\omega^2-(\gamma_j^E)^2}\sum_{n=1}^{N}\frac{\tilde{\varphi}_j(\mathbf{r}_n^S)}{\Lambda_j}\frac{Q_n^S}{Q^S}}_{\text{Contribution of primary sound field}} - \underbrace{\frac{\left[\frac{\omega^2}{\omega^2-(\gamma_j^E)^2}\frac{\varphi_j(\mathbf{r}^R)}{\Lambda_j}\right]\left(i\frac{z_0}{kZ}\frac{1}{V^E}\right)\sum_{h=1}^{J}\left[\frac{\omega^2}{\omega^2-(\gamma_h^E)^2}\frac{\varphi_h(\mathbf{r}^R)}{\Lambda_h}\sum_{n=1}^{N}\tilde{\varphi}_h(\mathbf{r}_n^S)\frac{Q_n^S}{Q^S}\right]}{1+i\frac{z_0}{kZ}\frac{1}{V^E}\sum_{h=1}^{J}\frac{\omega^2}{\omega^2-(\gamma_h^E)^2}\frac{[\varphi_h(\mathbf{r}^R)]^2}{\Lambda_h}}}_{\text{Contribution of acoustic resonator}}. \tag{10}$$

The first term on the right-hand side of Eq. (10) is the contribution of the primary sound field and the second term results from inserting an acoustic resonator into the enclosure. Note that a maximum $\varphi_j(\mathbf{r}^R)$ would not automatically warrant a maximum performance of the absorber. If the resonator is located in the node of the mode [i.e., $\varphi_j(\mathbf{r}^R)=0$], the value of the second term is systematically zero, suggesting zero contribution to the jth modal response. From Eq. (10) it can also be observed that the noise control is a result of the second part on the right-hand side of the equation, i.e., the acoustic interaction between the enclosure and the resonator. A strong acoustic interaction between the enclosure and the

resonator can provide good noise control, which depends on the location of $\mathbf{r}^R$ and the physical parameters of the resonator indicated in Z. Through optimizing the location and physical parameters of the resonator, we can maximize the acoustic interaction in the second term of Eq. (10), and thus obtain optimal noise control.

When only the targeted mode, i.e., the jth enclosure mode, is dominant, Eq. (10) can be simplified by ignoring all other minor enclosure modes as

$$\frac{P_j}{\frac{Q^S}{k^2V^E}} = \frac{1}{1+i\frac{z_0}{kZ}\frac{1}{V^E}\frac{\omega^2}{\omega^2-(\gamma_j^E)^2}\frac{[\varphi_j(\mathbf{r}^R)]^2}{\Lambda_j}}\left(\frac{P_j}{\frac{Q^S}{k^2V^E}}\right)_{\text{without resonator}}, \tag{11}$$

where

$$\left(\frac{P_j}{\frac{Q^S}{k^2V^E}}\right)_{\text{without resonator}} = \frac{\omega^2}{\omega^2-(\gamma_j^E)^2}\sum_{n=1}^{N}\frac{\tilde{\varphi}_j(\mathbf{r}_n^S)}{\Lambda_j}\frac{Q_n^S}{Q^S} \tag{12}$$

is the jth modal response of the enclosure in the absence of the resonators.

Equation (11) is consistent with that shown in Ref. 12. It is more clearly shown in Eq. (11) that when inserting an acoustic resonator at $\mathbf{r}^R$ that targets the jth enclosure mode, the jth modal response is reduced by the factor of

$$1/1+i\frac{z_0}{kZ}\frac{1}{V^E}\frac{\omega^2}{\omega^2-(\gamma_j^E)^2}\frac{[\varphi_j(\mathbf{r}^R)]^2}{\Lambda_j}.$$

From this simplified case, it is seen that when the physical parameters of the resonator are already determined, the control result can be optimized only if the resonator is located at any of the antinodes of the targeted mode. However, the actual case is much more complex than the simplified one because the resonator is coupled to all enclosure modes, not just to the targeted or dominant one. This particular issue will be discussed later in this paper.

The volume velocity source strength Q^R directed outwards from the resonator into the enclosure can be derived based on Eq. (3), $p(\mathbf{r},t)=-\rho_0\dot{\phi}(\mathbf{r},t)$, $\phi(\mathbf{r},t)=\Sigma\psi_j(t)\varphi_j(\mathbf{r})$, and Eq. (10) as

$$\frac{Q^R}{Q^S} = -\frac{i\frac{z_0}{kZ}\frac{1}{V^E}\sum_{h=1}^{J}\left[\frac{\omega^2}{\omega^2-(\gamma_h^E)^2}\frac{\varphi_h(\mathbf{r}^R)}{\Lambda_h}\sum_{n=1}^{N}\tilde{\varphi}_h(\mathbf{r}_n^S)\frac{Q_n^S}{Q^S}\right]}{1+i\frac{z_0}{kZ}\frac{1}{V^E}\sum_{h=1}^{J}\frac{\omega^2}{\omega^2-(\gamma_h^E)^2}\frac{[\varphi_h(\mathbf{r}^R)]^2}{\Lambda_h}}. \tag{13}$$

It is seen that the volume velocity source strength out of the resonator aperture depends not only on the acoustic output impedance of the resonator itself, but also on all acoustic modes of the enclosure. In terms of volume velocity source strengths, the modal response shown in Eq. (10) can be rewritten as

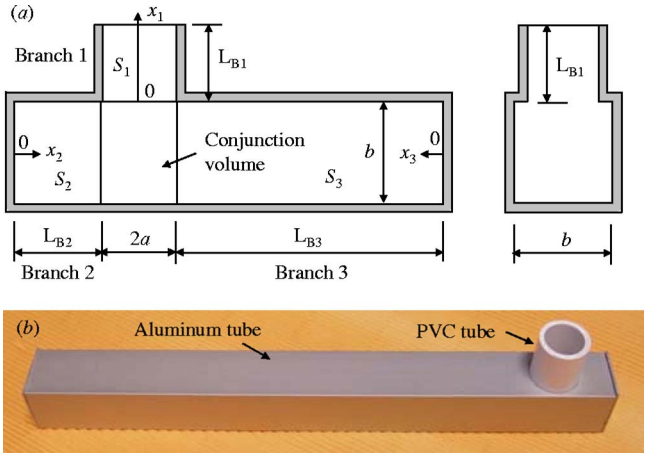

FIG. 1. (Color online) A typical T-shaped acoustic resonator: (a) Design geometries and (b) a fabricated TAR.

$$\frac{P_j}{\frac{Q^S}{k^2V^E}} = \underbrace{\frac{\omega^2}{\omega^2-(\gamma_j^E)^2}\sum_{n=1}^{N}\left[\frac{\tilde{\varphi}_j(\mathbf{r}_n^S)}{\Lambda_j}\frac{Q_n^S}{Q^S}\right]}_{\text{Contribution of primary sound field}} + \underbrace{\frac{\omega^2}{\omega^2-(\gamma_j^E)^2}\frac{\varphi_j(\mathbf{r}^R)}{\Lambda_j}\frac{Q^R}{Q^S}}_{\text{Contribution of accoustic resonator}}. \tag{14}$$

Therefore, the analytical solution of the sound pressure inside the enclosure is represented as

$$\frac{p(\mathbf{r})}{\frac{i\rho_0\omega Q^S}{k^2V^E}} = \underbrace{-\sum_{h=1}^{J}\left[\frac{\omega^2}{\omega^2-(\gamma_h^E)^2}\frac{\varphi_h(\mathbf{r})}{\Lambda_h}\sum_{n=1}^{N}\tilde{\varphi}_h(\mathbf{r}_n^S)\frac{Q_n^S}{Q^S}\right]}_{\text{Contribution of primary sound field}} \underbrace{-\sum_{h=1}^{J}\left[\frac{\omega^2}{\omega^2-(\gamma_h^E)^2}\frac{\varphi_h(\mathbf{r})\varphi_h(\mathbf{r}^R)}{\Lambda_h}\frac{Q^R}{Q^S}\right]}_{\text{Contribution of acoustic resonator}}. \tag{15}$$

C. Acoustic output impedance of TAR

In the above-mentioned derivations, the acoustic output impedance of a resonator was used to characterize the dynamic behavior of the secondary sound source. In this section, the expression of the acoustic output impedance for T-shaped acoustic resonators is derived.

A typical TAR[7,8,11] is shown in Fig. 1. The resonator consists of three branches—1–3—as depicted in Fig. 1. Branch 1 is a circular tube having radius a and physical length L_{B1}, and Branches 2 and 3 are coaxial and have cross-sectional areas S_2 and S_3 (circular or rectangular) and physical lengths L_{B2} and L_{B3}, respectively. Branch 1 is perpendicular to Branches 2 and 3. It is assumed that the wave inside the TAR is a plane wave, which is satisfied in this study since the sound wavelength of interest is sufficiently larger than the largest cross-sectional dimension of the resonators. When ignoring the absorptive process within the fluid and at the walls of the resonator, the acoustic output impedance, Z, at the external aperture of the TAR can be obtained from Ref. 11 as

$$Z = iz_0 \frac{1 - \frac{S_2}{S_1}\tan(k_1L_1)\tan(k_2L_2) - \frac{S_3}{S_1}\tan(k_1L_1)\tan(k_3L_3)}{S_1\tan(k_1L_1) + S_2\tan(k_2L_2) + S_3\tan(k_3L_3)}, \tag{16}$$

where k_1, k_2, and k_3 are the wave numbers of three branches, composed of three tube segments (the three wave numbers are equal when the internal dissipation is not considered), and L_1, L_2, and L_3 are the effective lengths of Branch 1, Branch 2, and Branch 3, respectively, which can be computed using the physical lengths by adding end corrections. When the external aperture of Branch 1 is unflanged, the hybrid end corrections of Branches 1, 2, and 3 presented in Refs. 7 and 11 are used,

$$\Delta L_1 = \frac{8}{3\pi}a, \tag{17}$$

$$\Delta L_2 = 1.5\frac{8}{3\pi}a, \tag{18}$$

$$\Delta L_3 = 1.5\frac{8}{3\pi}a. \tag{19}$$

The absorptive process within the fluid and at the walls of a resonator is important because it provides a damping (internal resistance) mechanism for the resonator, which prevents the resonator from producing a mathematical singularity at its resonance frequencies. The absorptive process directly dissipates the input energy. The remaining, nondissipated energy is reradiated back to the enclosure from the resonator aperture as the secondary sound source, resulting in acoustic interaction with the primary source. When the internal resistance of the resonator is very small, the acoustic interaction between the enclosure and resonator sharply splits the targeted resonance peak of the enclosure into two parts, and the peak response is significantly attenuated within a very narrow frequency band.[4] By properly increasing the internal resistance of the coupled resonator mode, the working bandwidth of the resonator can be improved, while sacrificing some control performance due to decreased amplitude. However, if the resistance is too large, both the velocity amplitude of the fluid inside the resonator and the strength of volume velocity out of the resonator aperture become too small; such low velocities can only produce low dissipation in the resonators and slight acoustic interaction between the enclosure and resonators and hence result in insignificant control at the targeted enclosure resonances. A resonator with optimally designed internal resistance can provide a good control performance in a relatively large working frequency bandwidth, which will be addressed in another paper.

If the absorptive process within the fluid and at the walls of the resonator is considered, we can replace the lossless wave number k_i $(i=1,2,3)$ in Eq. (16) by a complex propagation constant $\mathbf{k}_i$, which can be approximately expressed with a dispersion relation[15]

$$\mathbf{k}_i = (k + \alpha_i) - i\alpha_i, \tag{20}$$

where $\alpha_i \ll k$ is the absorption coefficient of tube i defined in Ref. 15. For each tube segment, it can be computed by

$$\alpha_i = \sqrt{\frac{\omega\mu}{8cz_0}}\left(1 + \frac{\gamma - 1}{\sqrt{P_r}}\right)\frac{L_i^P}{S_i}, \tag{21}$$

where μ is the shear viscosity coefficient, γ is the specific heat ratio, $P_r = \mu C_p/\kappa$ is the Prandtl number of the medium, C_p is the specific heat at constant pressure, κ is the thermal conduction coefficient, and L_i^P and S_i are the inner-perimeter and cross-sectional area of tube i, respectively.

When considering absorption, the tangent function used in Eq. (16) is extended as[14]

$$\tan[(k + \alpha_i) - i\alpha_i]L_i = \frac{\sin^2(k + \alpha_i)L_i\cosh^2\alpha_iL_i + \cos^2(k + \alpha_i)L_i\sinh^2\alpha_iL_i}{\cos(k + \alpha_i)L_i\sin(k + \alpha_i)L_i + i\sinh\alpha_iL_i\cosh\alpha_iL_i}. \tag{22}$$

D. Sequential design method using acoustic resonators

When using acoustic resonators to control noise in a small enclosure, a SDM is proposed as follows.

(1) A TAR to target the desired enclosure mode at $\omega^R = ck^R$ is designed and fabricated using[11]

$$L_3 = \frac{\operatorname{atan}\left(\frac{S_1}{S_3}\cot(k^RL_1) - \frac{S_2}{S_3}\tan(k^RL_2)\right) + (i-1)\pi}{k^R}, \tag{23}$$

where L_1, L_2, S_1, S_2, and S_3 are given, and $i(=1,2,3,4,\ldots)$ are the harmonics of the acoustic resonator. Any resonator harmonics can be used for control.

(2) The optimal location of TAR is determined while accounting for multiple enclosure modes.

When there is a single resonator inside the enclosure and only the targeted enclosure mode φ_j is dominant, Eq. (11), it is known that a maximal noise control can be obtained only if the resonator is located at any antinode of the targeted mode.[12] However, this result is not true when multiple modes are taken into account in the acoustic coupling model. Actually, the resonator does couple with all acoustic modes of the enclosure.[12] Therefore, there exists an optimal location for the resonator among antinodal points, in which the best control performance of the resonator can be obtained. For controlling sound pressure at a specific point, the optimal location can be determined through comparing the SPL obtained from different resonator locations. The optimal location corresponds to the largest SPL reduction in the vicinity of the targeted frequency.

(3) After coupling the lightly damped TAR with the lightly damped enclosure, two new resonance peaks appear to replace the original peak, and a frequency shift at other nontargeted resonances also occurs. In order to improve the control performance, new resonators can be added to tackle the newly emerged peaks by repeating steps (1) and (2).

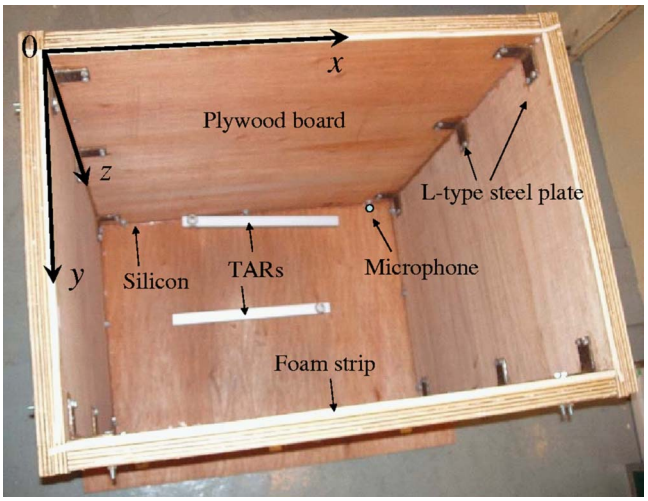

FIG. 2. (Color online) Right parallepiped reverberant enclosure with a coordinate system.

Theoretically, provided that enough space is available to host additional resonators, the sound pressure level at the targeted resonance can be reduced to a desired level after several iterations.

III. COMPARISONS BETWEEN THEORY AND EXPERIMENT

The noise control of an enclosure using multiple TARs was numerically investigated and experimentally validated. To this end, one right parallelpiped reverberant enclosure having geometric dimensions l_x=0.976 m, l_y=0.695 m, and l_z=1.188 m was used and shown in Fig. 2. The enclosure was fabricated using six plywood boards assembled with L-type steel plates, bolts, and nuts (see Fig. 2). Each of the six boards was comprised of two 1-in. boards, which were tightly screwed together. Silicon sealant and foam strips were also applied to prevent air leakage from the enclosure. The upper enclosure wall was removable and an enclosed loudspeaker was located on the upper surface at (100,59, −51) mm to excite the primary sound field in the enclosure through a square hole of 100×100 mm. The SPL at an arbitrary point (816,70,1028) mm in the enclosure was predicted and measured. In all simulations, a total of 216 enclosure modes were used [$(l,m,n)=(0\sim5,0\sim5,0\sim5)$, where l,m,n are the node number in x, y, and z direction, respectively.]. The eigenfunctions $\varphi_j(\mathbf{r}^R)$ of the enclosure accounting for the thermalviscous boundary conditions were obtained from Ref. 13, and the eigenvalues $\omega_j^E=\omega_j+iC_j$ were assembled using the undamped natural frequency of the jth enclosure mode ω_j and the jth *ad hoc* damping coefficient $C_j=\omega_j/2Q_j$, obtained from the measured quality or Q factors listed in Table I. All physical parameters of air, tabulated in Table II, were used in the simulations. The T-shaped acoustic resonators used in the simulations and experiments had a circular cross-sectional Branch 1, 21 mm in internal diameter, and square cross-sectional Braches 2 and 3 that were 29.5×29.5 mm. The physical lengths of Branch 1 and Branch 2 were L_{B1}=30 mm and L_{B2}=20 mm, respectively, and the physical length of Branch 3 was calculated with Eq. (23). In this study, the desired working frequency of all TARs was chosen to be their fundamental or Helmholtz frequency [i=1 in Eq. (23)]. No damping materials were used inside the resonator, and only the thermalviscous boundary conditions were considered.

TABLE I. Computed natural frequencies and measured Q factors of the enclosure.

Index	Mode number (lmn)	Natural frequency (Hz)	Q factor
1	000	0	⋯
2	001	145.0	32
3	100	176.5	42
4	101	228.4	44
5	010	247.8	46
6	011	287.1	84
7	002	290.0	42
8	110	304.3	51
9	111	337.0	79
10	102	339.5	60
11	200	353.0	80
12	012	381.5	60
13	201	381.6	45
⋯	⋯	>400.0	45

For the simulations, the convergence of the model size was achieved by examining the volume velocity at the resonator aperture of TARs and the pressure inside the enclosure as the number of enclosure modes was gradually increasing. When the number of the enclosure modes was varied from 216 ($l=m=n=0-5$) to 1000 ($l=m=n=0-9$), neither the volume velocity nor the pressure at (816,70,1028) mm in the enclosure, as predicted by Eq. (6), were found to change (not shown). As a result, 216 enclosure modes were determined to be for the model size.

A. Evaluation of dissipation characteristics of resonators

Equation (16) was used to calculate the acoustic impedance of TARs, based on the absorption coefficient of each tube segment using Eq. (21). It is known that the damping of a resonator is an important parameter, which significantly affects both the coupled amplitude at the targeted resonance peak of the enclosure and the working frequency bandwidth of the resonator itself. Therefore, the validity of Eq. (21)

TABLE II. Air properties.

Physical parameter	Used value
Ambient temperature, T (°C)	20
Humidity (%)	90
Speed of sound, c (m/s)	344.5
Density of air, ρ_0 (kg/m^3)	1.205
Specific heat ratio of air, γ	1.402
Thermal conductivity of air, κ [W/(m K)]	0.0257
Specific heat at constant pressure of the air, C_p [J/(kg K)]	1.005×10^3
Coefficient of shear viscosity, μ (Pa s)	1.88×10^{-5}

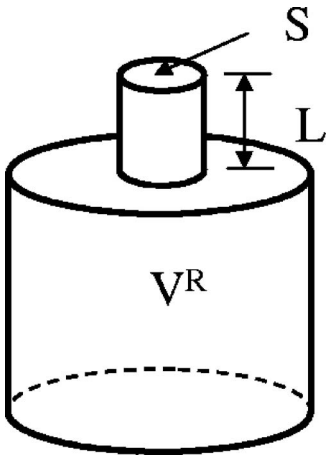

FIG. 3. A classical Helmholtz resonator.

should first be assessed. To this end, a classical Helmoholtz resonator shown in Fig. 3 is used, since a simple relationship exists between the absorption coefficient and the measurable Q factor. Therefore, it provides an alternative way to validate the absorption coefficient predicted by Eq. (21) using measured data. This relationship is derived as follows.

The acoustic output impedance of a Helmholtz resonator can be derived as

$$Z = \frac{z_0}{ikV^R A^R}, \tag{24}$$

where

$$A^R = \frac{(k^R)^2}{k^2 - iRk - (k^R)^2} \tag{25}$$

is the acoustic parameter of the Helmholtz resonator, V^R the volume of the resonator body, $R = R_w/\rho_0 cL$, L the effective neck length counting the exterior and interior end correction, and R_w the internal resistance in the resonator neck excluding the external radiation resistance, which can be computed from the measured Q factor, Q_R, and the resonance frequency ω^R of the resonator by $R_w = \omega^R \rho_0 L/Q_R$.[12]

Using the complex propagation constant $\mathbf{k}$, A^R can be also represented as

$$A^R = \frac{(k^R)^2}{\mathbf{k}^2 - (k^R)^2}. \tag{26}$$

When the medium is air, the absorption coefficient of an empty-necked resonator is very low at low frequencies, thus the complex propagation constant can be approximately expressed as $\mathbf{k} = k - i\alpha$.[14] Substituting this result into Eq. (26), expanding, and ignoring the higher-order term α^2 $(\alpha \ll 1)$ gives

$$A^R \approx \frac{(k^R)^2}{k^2 - i2\alpha k - (k^R)^2}. \tag{27}$$

Comparing Eq. (27) with Eq. (25), the internal resistance can be estimated as

$$R_w \approx 2\rho_0 cL\alpha. \tag{28}$$

Substituting $R_w = \omega^R \rho_0 L/Q_R$ into Eq. (28), the absorption coefficient of the Helmholtz resonator at its resonance frequency can be expressed in terms of the measured Q factor and resonance frequency ω^R as

$$\alpha(\omega = \omega^R) \approx \frac{\omega^R}{2cQ_R}. \tag{29}$$

For experimental validation, three resonators named HR1, HR2, and HR3 were fabricated using circular cross-sectional PVC tubes. The geometric dimensions are listed in Table III. The measured resonance frequencies, Q factors, and the predicted absorption coefficients using Eqs. (21) and (29) are also shown in Table III. It can be seen that the predicted absorption coefficients using Eq. (21) are slightly smaller than the experimentally estimated ones, with errors ranging from 6% to 9%. Generally speaking, the agreement between the model and experimental data is satisfactory. Therefore, it is concluded that Eq. (16) can be used to calculate the acoustic impedance of the TAR using Eq. (21).

TABLE III. Measured and predicted absorption coefficients.

Helmholtz resonator	Dimensions (mm)	Measured resonance freq. (Hz)	Measured Q factor	Measured absorption coefficient Eq. (29)	Predicted absorption coefficient Eq. (21)	Error (%)
HR1	Neck diameter 21 Neck length 60.0 Body diameter 77.5 Body length 155.3	136.0	35.3	0.035	0.033	6
HR2	Neck diameter 21 Neck length 79.2 Body diameter 79.2 Body length 65.3	222.0	43.5	0.047	0.043	9
HR3	Neck diameter 21 Neck length 50.4 Body diameter 77.5 Body length 57.5	245.6	47.1	0.048	0.045	6

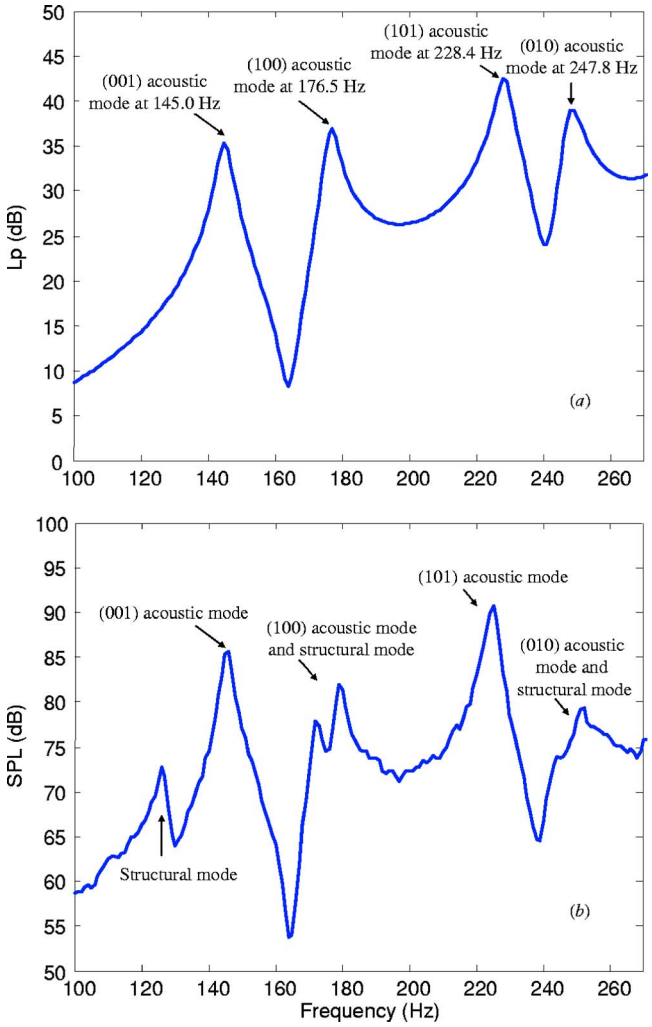

FIG. 4. (Color online) Predicted and measured baseline SPLs at (816,70,1028) mm: (a) Predicted and (b) measured.

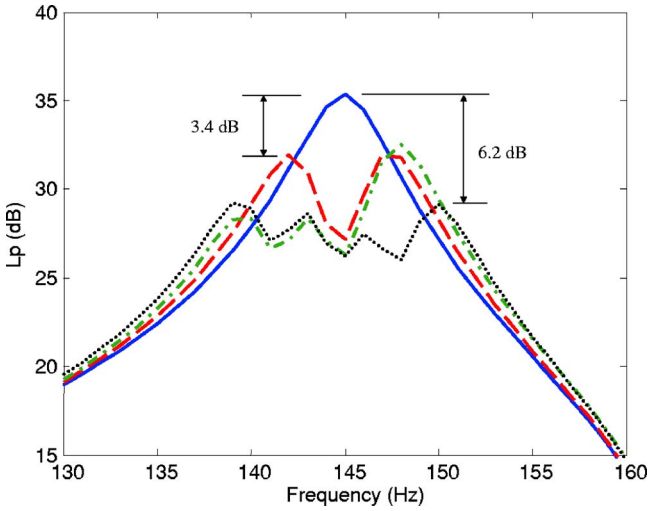

FIG. 5. (Color online) Predicted SPLs at (816,70,1028) mm:(—) Without resonator; (---) with TAR_145; (-·-) with TAR_145 and TAR_142; and (···) with TAR_145, TAR_142, and TAR_148.

B. Theoretical and experimental control results

In this section, the capability of the proposed SDM to tackle SPL reduction using a TAR array comprised of six TARs at two resonance frequencies is theoretically and experimentally demonstrated. First, the baseline SPL without resonators was predicted and compared with the measured baseline to validate the current theory. Second, the implementation of the SDM for noise control was illustrated in detail. Finally, the optimal location predicted for a 145 Hz TAR was experimentally validated.

1. Predicted and measured baseline SPL

The predicted and measured baseline SPLs without TARs are shown in Figs. 4(a) and 4(b), respectively. Notice that due to the difficulty in determining the volume velocity source strength Q^S for the primary sound source, numerical results are obtained in terms of $p(\mathbf{r})/(i\omega\rho_0 Q^S/k^2V^E)$. Therefore, the predicted SPL cannot be directly compared with the measured SPL. Instead, comparison will focus on the general trends and frequency-dependent variations for the sound pressure inside the enclosure. This is a common practice widely used in previous studies such as in Cummings.[13] The agreement between the predicted and measured results in this ideal condition (rigid walls) is obvious. Both curves undergo very similar global variations with respect to frequency. A more detailed inspection of the predicted SPL curve shows four major peaks at 145.0, 176.5, 228.4, and 247.8 Hz in the frequency band [100,270] Hz. The same peaks can also be found in the measured curve near these four locations. The experimental curve also shows two additional small peaks at 123.0 and 176.5 Hz. Since the wooden boards used to fabricate the enclosure walls are not fully rigid, the first peak at 123.0 Hz is a structural resonance that has been identified by substantial measurements, and the second peak at 176.5 Hz is a coupled structural-acoustic mode. This structural-acoustic coupling also affects the peak values around 247.8 Hz. Therefore, only two significant peaks were clearly identified from the measured baseline data: one at 145 Hz, having SPL 86 dB, which is dominated by the acoustic mode (001), and another at 224 Hz with SPL 91 dB, which is governed by the acoustic mode (101). While the measured (001) mode exactly matches the prediction, the predicted resonance frequency of 228.4 Hz for the (101) mode differs slightly from the measured peak at 224 Hz. The two peaks at 145 and 228 Hz will be targeted in the following noise control analyses.

2. Predicted and measured control results

The SDM procedure was implemented to control noise at the two resonance peaks at 145 and 228 Hz as follows. First, to reduce the noise level at the peak of 145 Hz, a TAR named TAR_145 was designed using Eq. (23). Note that the resonator was named using a "TAR_" and an integer indicating the resonator's Helmholtz frequency. The optimal location of TAR_145 was determined according to a procedure that will be addressed in Sec. III B 3. The theoretical SPL curve at (816,70,1028) mm with TAR_145 is shown in Fig. 5 by a dashed line. After introducing TAR_145, a 3.4 dB SPL reduction was achieved, and the original resonance peak at 145 Hz was replaced by two new peaks corresponding to two new-coupled frequencies at 142 and 147 Hz due to

TABLE IV. Parameters and optimal locations of TARs.

Resonator	Helmholtz frequency (Hz)	Branch 1 diameter (mm)	Branches 2 and 3 width × height (mm)	L_{B1} (mm)	L_{B2} (mm)	L_{B3} (mm)	Predicted location (mm)
TAR_145	145	21	29.5×29.5	30	20	482.4	(700, 400, 1128)
TAR_142	142	21	29.5×29.5	30	20	495.0	(300, 0, 1128)
TAR_148	148	21	29.5×29.5	30	20	470.4	(200, 200, 60)
TAR_229	228	21	29.5×29.5	30	20	265.7	(0, 300, 60)
TAR_224	224	21	29.5×29.5	30	20	272.5	(900, 500, 1128)
TAR_233	233	21	29.5×29.5	30	20	257.5	(800, 200, 1128)
TAR_177	177	21	29.5×29.5	30	20	374.9	(0, 0, 1128)
TAR_173	173	21	29.5×29.5	30	20	386.1	(916, 0, 110)
TAR_180	179.5	21	29.5×29.5	30	20	368.1	(60,0,0)
TAR_249	249	21	29.5×29.5	30	20	233.7	(100,60,0)

acoustic interaction. In order to further reduce the SPL around 145 Hz, another TAR named TAR_142 was designed to target the new peak at 142 Hz. Its optimal location was determined after TAR_145 was installed. The computed SPL with installed TAR_145 and TAR_142 is also shown in Fig. 5 by a dot-dashed line. From the curve, it is observed that the old peak at 147 Hz shifts to 148 Hz due to the new acoustic coupling with TAR_142. Thus, a TAR with Helmholtz frequency 148 Hz and named TAR_148 was inserted. The predicted SPL with a total of three TARs are again shown in Fig. 5 by a dotted line. This leads to a total of 6.2 dB SPL reduction in the enclosure mode at 145 Hz. The geometric dimensions of the three TARs and predicted optimal locations are listed in Table IV. These TARs were also fabricated and tuned for experimental validations. The measured SPL curves with and without TARs are shown in Fig. 6, showing 5.0 dB SPL reduction with only TAR_145 installed and 7.8 dB reduction with three resonators. Comparisons between Figs. 5 and 6 show very similar SPL variation for each configuration. Quantitatively speaking, the predicted SPL reductions are smaller than the measured ones and the predicted peaks are also sharper than the measured peaks. One plausible explanation may be that the real absorption coefficients of the resonators are slightly larger than the predicted ones using Eq. (21), which is in agreement with the observations made in Sec. III A and summarized in Table III.

To further control the peak at 228 Hz, another three TARs were designed and implemented by following the same methodology. The three resonators, TAR_228, TAR_224, and TAR_233, were added one after another at their corresponding optimal locations determined by the model. The final resonator array was comprised of six TARs that simultaneously control the two resonance peaks at 145 and 228 Hz. Their geometric dimensions, working frequency, and optimal locations are also listed in Table IV. Figure 7 shows the predicted SPLs with and without the resonator array. A 5.9 and 7.4 dB reduction in SPL around frequencies 145 and 228 Hz is predicted, respectively. Notice that the total volume occupied by all six resonators is 0.0022 m^3, which is only 0.3% of the enclosure volume 0.833 m^3. Therefore the effect of the physical presence of the resonators inside the enclosure is negligible.

The final configuration using all six resonators was also experimentally tested. Resonators (TAR_145, TAR_142, TAR_148, TAR_224, TAR_220, and TAR_228) were installed

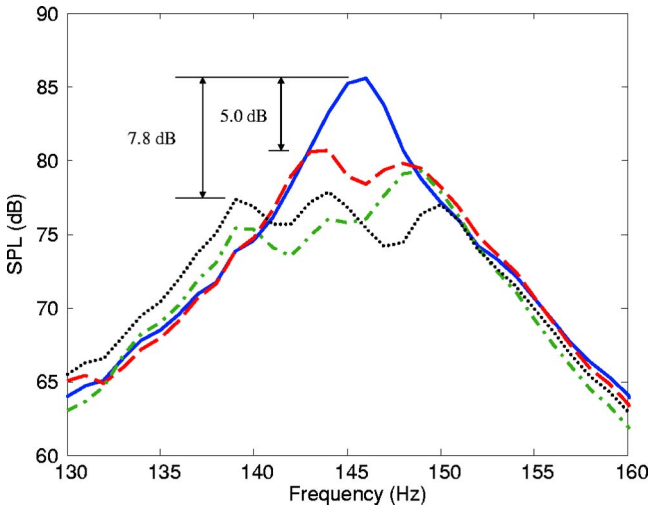

FIG. 6. (Color online) Measured SPLs at (816,70,1028) mm:(—) Without resonator; (---) with TAR_145; (---) with TAR_145 and TAR_142; and (···) with TAR_145, TAR_142, and TAR_148.

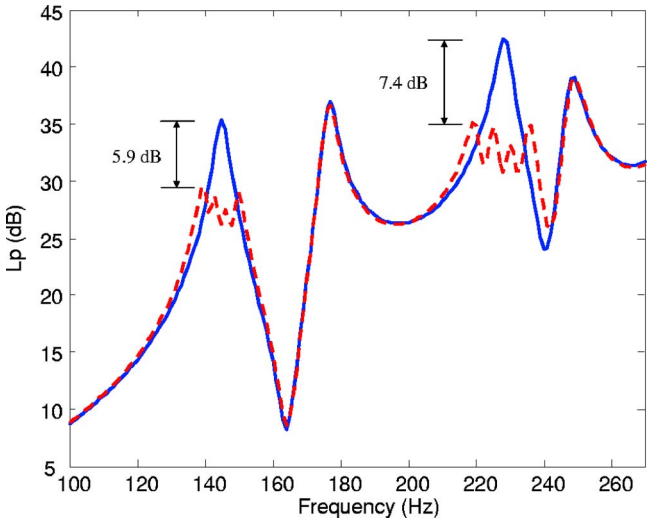

FIG. 7. (Color online) Predicted SPLs at (816,70,1028) mm:(—)Without resonator; and (---) with TAR_145, TAR_142, TAR_148, TAR_228, TAR_224, and TAR_233.

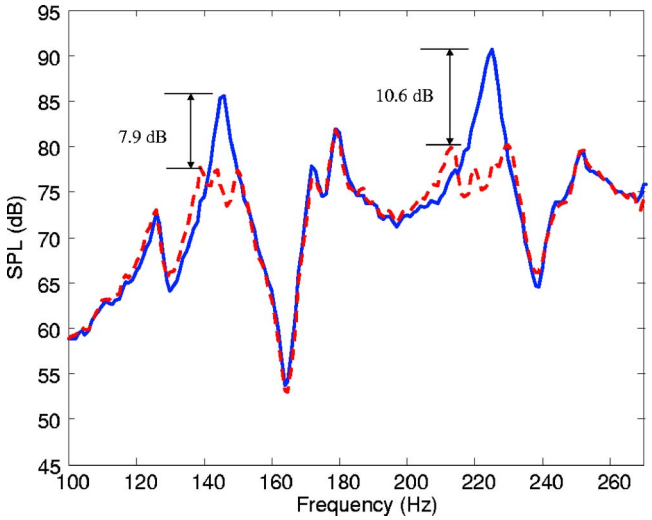

FIG. 8. (Color online) Measured SPLs at (816,70,1028) mm: (—) Without resonator; and (---) with TAR_145, TAR_142, TAR_148, TAR_224, TAR_220, and TAR_228.

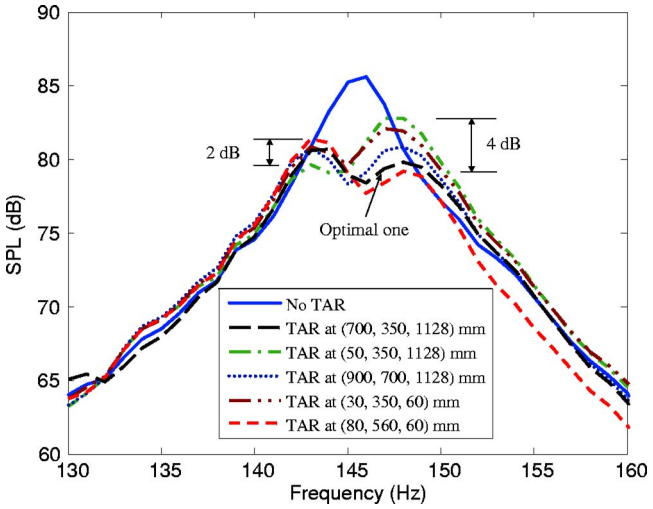

FIG. 9. (Color online) Measured representative SPL curves for identifying optimal location of the resonator TAR_145.

at locations determined by the model. The measured SPL with and without the TAR array is shown in Fig. 8. SPL reductions of 7.9 and 10.6 dB were observed around 145 and 224 Hz, respectively. Compared to the predicted results shown in Fig. 7, a remarkable resemblance in the control results can be observed, testifying to the validity of the proposed design model and methodology.

3. Predicted and measured optimal locations of TARs

Theoretical analysis in Sec. II suggests that the optimal location of a TAR is not an arbitrary point among all possible antinode points because each resonator couples with all enclosure modes. When determining the optimal location for a TAR, the interaction of the resonator with multiple enclosure modes, in addition to the targeted mode, must be considered. The proposed model actually provides such a tool. Assuming that possible locations for installing resonators are constrained near the six-wall surfaces of the enclosure, which are: $x=60$ mm (equal to the physical length of resonator Branch 1 plus the external cross-sectional height of the resonator Branch 2 or 3), $x=l_x-60$ mm, $y=60$ mm, $y=l_y-60$ mm, $z=60$ mm, and $z=l_z-60$ mm, a grid with a step of 100 mm in each direction was created for each surface, the frequency step is 1 Hz, and the SPL curves were computed for each TAR location at each grid point. After comparing the SPLs for all locations, the optimal one that provides the maximum SPL reduction in the vicinity of the targeted resonance frequency was chosen. Applying this procedure to a TAR_145, the optimization location was determined to be (700,400,1128) mm, with a corresponding SPL reduction of 3.4 dB around the targeted frequency of 145 Hz.

An experimental validation on this particular point was carried out. A series of measurements were conducted when the resonator was located at different locations. Five representative measured SPL curves are shown in Fig. 9, which shows a variation range of roughly 4 dB in terms of peak values among the five configurations. The experimentally determined optimal location at (700,400,1128) nm matches exactly the one predicted by simulations.

C. Theoretical design of a wide range control

This last example illustrates the capability of the proposed design approach in achieving wide band (or multiresonance) control using a resonator array, which consisted of ten TARs, including the six TARs used earlier and other four new TARs, named TAR_177, TAR_173, TAR_180, and TAR_249. Based on the control achieved in Sec. III B 2, the four new resonators were respectively designed and optimally positioned using SDM. The geometric dimensions of the four resonators and their predicted optimal locations are again listed in Table IV. The predicted SPL curves with and without the ten resonators are shown in Fig. 10. It can be seen that all four major resonances at 145, 177, 229, and 249 Hz can be simultaneously targeted, resulting in sound

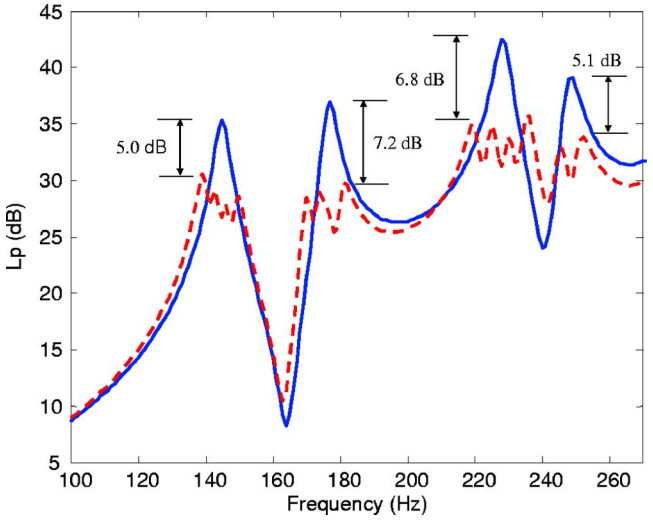

FIG. 10. (Color online) Predicted SPL curves at (816,70,1028) mm for demonstrating wide range control in the first four resonance peaks using ten TARs: (—) Without resonator; and (---) with resonators.

pressure level reduction ranging from 5.0 to 7.2 dB. Therefore, at the expense of adding more resonators, significant wide band control can be achieved.

IV. CONCLUSIONS

A theoretical model to predict the acoustic performance of multiple resonators placed in an acoustic enclosure and a reliable design methodology to maximize the control performance have been presented and experimentally validated. The sound field inside the enclosure with integrated acoustic resonators is a result of primary sound sources and the secondary sound sources formed from reradiation of the resonators, where the latter is the resonator response to the excitation from the enclosure. All these phenomena occur as a result of the acoustic interaction as a whole, which is significantly affected by the location of the resonators. The optimal location of the resonator to ensure strong interaction between the enclosure and the resonator is no longer an arbitrary point in the antinodal surface, as suggested by previous studies that only considered the interaction between the single targeted mode and the resonator. With the consideration of all possible coupled modes, the optimal location of a resonator can be determined using the general approach proposed in this paper, which is based on a general coupling model. This technique becomes a necessity when multiple resonators are used either to increase the sound reduction performance or to achieve wide range control.

The acoustic interaction is also affected by the internal resistance or the absorption coefficient of the resonator. It is found that the internal resistance of the resonator not only determines the energy dissipation inside the resonator, but also the source strength of the volume velocity directed out of the resonator aperture, and further influences the acoustic coupling with the enclosure. An optimally designed internal resistance can increase energy dissipation and improve bandwidth of the resonator around its working frequency.

A simulation model and a systematic design approach are established and validated by experiments. It is shown that, with the help of the proposed design methodology, either single or multiple resonance peaks of the enclosure can be successfully controlled.

ACKNOWLEDGMENTS

The authors wish to acknowledge a grant from Research Grants Council of Hong Kong Special Administrative Region, China (Project No. PolyU 5137/06E) and support by the Central Research Grant of The Hong Kong Polytechnic University through Grant No. G-YE67.

[1] J. M. Mason and F. J. Fahy, "The use of acoustically tuned resonators to improve the sound transmission loss of double-panel partitions," J. Sound Vib. **124**, 367–379 (1988).
[2] S. J. Estève and M. E. Johnson, "Reduction of sound transmitted into a circular cylindrical shell using distributed vibration absorbers and Helmholtz resonators," J. Acoust. Soc. Am. **112**, 2840–2848 (2002).
[3] S. J. Estève and M. E. Johnson, "Reduction of sound transmitted into a composite cylinder using distributed vibration absorbers and Helmholtz resonators," J. Vibr. Acoust. **112**, 2040–2048 (2002).
[4] S. Griffin, S. A. Lane, and S. Huybrechts, "Coupled Helmholtz resonators for acoustic attenuation," J. Vibr. Acoust. **123**, 11–17 (2001).
[5] S. A. Lane, R. E. Richard, and S. J. Kennedy, "Fairing noise control using tube-shaped resonators," J. Spacecr. Rockets **42**, 640–646 (2005).
[6] D. Li and J. S. Vipperman, "On the noise transmission and control for a cylindrical ChamberCore composite structure," J. Sound Vib. **288**, 235–254 (2005).
[7] D. Li and J. S. Vipperman, "Noise control of mock-scale ChamberCore payload fairing using integrated acoustic resonators," J. Spacecr. Rockets **43**, 877–882 (2006).
[8] D. Li, "Vibroacoustic behavior and noise control studies of advanced composite structures," Ph.D. dissertation, School of Engineering, University of Pittsburgh, Pittsburgh, PA, 2003.
[9] E. Giampaoli and S. N. Y. Gerges, "Low frequency sound absorption by cavity resonator masonry blocks," Noise Control Eng. J. **33**, 131–138 (1989).
[10] V. H. Fuchs, "Alternative fibreless absorber- new tools and materials for noise control and acoustic comfort," Acta Acust. **87**, 414–422 (2001).
[11] D. Li and J. S. Vipperman, "On the design of long T-shaped acoustic resonators," J. Acoust. Soc. Am. **116**, 2785–2792 (2004).
[12] F. J. Fahy and C. Schofield, "A note on the interaction between a Helmholtz resonator and an acoustic mode of an enclosure," J. Sound Vib. **72**, 365–378 (1980).
[13] A. Cummings, "The effects of a resonator array on the sound field in a cavity," J. Sound Vib. **154**, 25–44 (1992).
[14] L. E. Kinsler, A. R. Frey, A. B. Coppens, and J. V. Sanders, *Fundamentals of Acoustics*, 4th ed. (Wiley, New York, 2000).
[15] A. D. Pierce, *Acoustics: An Introduction to its Physical Principles and Applications* (Acoustical Society of America, Melville, NY, 1989).